Sub-minute kinetics of human red cell fumarase: ^{1}H spin-echo NMR spectroscopy and ^{13}C rapid-dissolution dynamic nuclear polarization

Dmitry Shishmarev[1,2], Alan J. Wright[3], Tiago B. Rodrigues[3], Giuseppe Pileio[4], Gabriele Stevanato[4], Kevin M. Brindle[3], and Philip W. Kuchel[1*]

[1]*The University of Sydney, School of Life and Environmental Sciences, Sydney NSW 2006, Australia*

[2]*Australian National University, John Curtin School of Medical Research, Canberra ACT 2601, Australia*

[3]*University of Cambridge, Cancer Research UK Cambridge Institute, Li Ka Shing Centre, Cambridge CB2 0RE, United Kingdom*

[4]*University of Southampton, School of Chemistry, Southampton SO17 1BJ, United Kingdom*

[*]*Correspondence*: Professor Philip W. Kuchel
School of Life and Environmental Sciences
Molecular Bioscience Building (G08)
The University of Sydney
New South Wales 2006
Sydney, Australia
Phone: +61 (2) 9351 3709
Fax: +61 (2) 9351 4726
Email: philip.kuchel@sydney.edu.au

Running title: Kinetics of human red cell fumarase

Keywords: fumarase kinetics; fumarate; malate; human red blood cell; hyperpolarization; Michaelis-Menten model

Abbreviations: 23BPG, 2,3-biphosphoglycerate; *Ht*, hematocrit; MCMC, Markov chain Monte Carlo; NAD, nicotinamide adenine dinucleotide; PBS, phosphate buffered saline; RBC, red blood cell; RD-DNP, rapid-dissolution dynamic nuclear polarization; RMSD, root mean square deviation; S/N, signal-to-noise ratio

ABSTRACT

Fumarate is an important probe of metabolism in hyperpolarized magnetic resonance imaging and spectroscopy. It is used to detect the release of fumarase in cancer tissues, which is associated with necrosis and drug treatment. Nevertheless, there are limited reports describing the detailed kinetic studies of this enzyme in various cells and tissues. Thus, we aimed to evaluate the sub-minute kinetics of human red blood cell fumarase using NMR spectroscopy, and provide a quantitative description of the enzyme that is relevant to the use of fumarate as a probe of cell rupture.

The fumarase reaction was studied using time courses of ^{1}H spin-echo and ^{13}C-NMR spectra. ^{1}H-NMR experiments showed that the fumarase reaction in hemolysates is sufficiently rapid to make its kinetics amenable to study in a period of ~3 min, a timescale characteristic to hyperpolarized ^{13}C-NMR spectroscopy. The rapid-dissolution dynamic nuclear polarization (RD-DNP) technique was used to hyperpolarize [1,4-^{13}C]fumarate, which was injected into concentrated hemolysates. The kinetic data were analyzed using recently developed FmR_{α} analysis and modeling the enzyme reaction using Michaelis-Menten equations. In RD-DNP experiments, the decline of the ^{13}C-NMR signal from fumarate, and the concurrent rise-and-fall of that from malate, were captured with high spectral resolution and signal-to-noise ratio, which allowed robust quantification of fumarase kinetics. The obtained kinetic parameters indicate the potential contribution of hemolysis to the overall rate of the fumarase reaction when ^{13}C-NMR RD-DNP is used to detect necrosis in animal models of implanted tumors. The developed analytical procedures will be applicable to studies of other rapid enzymatic reactions using conventional and hyperpolarized-substrate NMR spectroscopy.

INTRODUCTION

Many biochemical processes in cells occur on the sub-minute timescale, making them notoriously difficult to record in situ. NMR spectroscopy has played a central role in our understanding of the kinetics of biochemical reactions in intact cells, with human erythrocytes (red blood cells; RBCs) being the most extensively studied mammalian cell-type. There are many comprehensive kinetic models of enzymatic pathways that were derived using NMR,[1-4] but such studies have been constrained by the need to acquire the spectral data over prolonged periods of time, with the metabolic system already in a quasi-steady state. The advent of rapid dissolution dynamic nuclear polarization (RD-DNP) enabled monitoring of metabolic conversions of individual ^{13}C-labeled compounds on the sub-minute timescale using ^{13}C-NMR spectroscopy in vivo,[5,6] in cell suspensions[7] or cell lysates, well before an equilibrated state of metabolite concentrations is established.

Fumarase (fumarate hydratase; EC 4.2.1.2) catalyzes the reversible hydration of fumarate to yield L-malate:

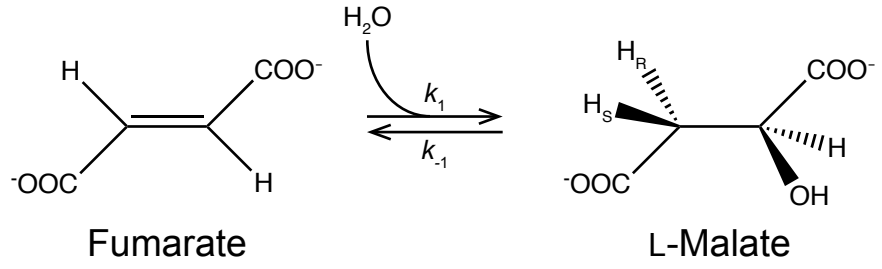

(1)

where k_1 and k_{-1} signify the apparent rate constants of the forward and reverse reactions, respectively. In the history of enzymology, fumarase occupies a special place due to its membership of the tricarboxylic acid (Krebs) cycle; accordingly, its reaction mechanism has been placed under intense scrutiny.[8-10]

Recently, fumarase has assumed a new significance as a diagnostic enzyme for tumor necrosis.[11] It is released into the interstitium of tumor nodules as the central cells become starved of oxygen and nutrients when their multiplication rate outstrips that of vascularization, or after the cells die from antineoplastic therapy. Since the entry of fumarate into cells is slow (the half-life for transport of 26 mM fumarate into RBCs is 11.1 ± 0.4 min),[12] the enzymatic conversion of hyperpolarized [1,4-^{13}C]fumarate in tumor-bearing mice, as detected on the sub-minute timescale by using RD-DNP, identifies necrosis in tumors in vivo.[11] Thus, it is possible to detect the response of malignant

tissues to chemotherapeutic agents, even before any change in the size of the tumor is apparent.[13] The fumarase reaction is well suited for such diagnostic experiments because it is rapid and does not require any cofactors, which simplifies its monitoring in cell lysates.

A notable feature of fumarase biochemistry is that there is only one copy of the corresponding gene in the human genome, and yet it has two primary intracellular locations;[14,15] one is expectedly in the mitochondria where the Krebs cycle is known to operate, and another is in the cytoplasm. The enzymes in the two locations are of exactly the same isoform. This raises a question about the role of the cytoplasmic enzyme; but, importantly for the present work, it helps explain why RBCs, which lack mitochondria, still possess fumarase activity.[16,17]

Based on this background knowledge, we aimed to: (**a**) re-evaluate the in situ kinetics of fumarase in freshly prepared human RBCs via time courses of ^{1}H spin-echo NMR spectra,[18] in order to assess the potential for kinetic characterization using RD-DNP; (**b**) record time courses in the very early stages of the fumarase-catalyzed reaction in hemolysates by using RD-DNP with [1,4-^{13}C]fumarate; (**c**) evaluate the performance of our recent FmR_{α} analysis[19] to the RD-DNP time courses (decay of the fumarate signal and rise-and-fall of the malate signal); and (**d**) estimate the values of the kinetic parameters in the Michaelis-Menten equations, used to model the forward and reverse reactions, with a Markov chain Monte Carlo (MCMC) fitting algorithm.[20] Such information will aid in discussions of the relative contribution of the RBC fumarase released from static hemolysed blood in necrotic tissue to that from the host tissue, for example, as occurs in tumor nodules after therapy.[11]

EXPERIMENTAL

Materials

All chemicals were purchased from Sigma Aldrich (North Ryde NSW, Australia; or Dorset, UK), unless otherwise stated. [1,4-^{13}C]fumaric acid was from Cambridge Isotopes (Tewksbury MA, USA). The trityl radical AH111501 was supplied by GE Healthcare (Little Chalfont, UK). The gadolinium chelate DOTAREM [Gd^{3+}2-(4,7,10-tris(carboxymethyl)-1,4,7,10-tetrazacyclododec-1-yl)acetate] was from Guerbet (Paris, France).

RD-DNP sample preparation

3.23 mmol of [1,4-^{13}C]fumaric acid was dissolved in 8.60 mmol of DMSO-d_6 with 11.8 μmol of trityl radical AH111501 and 0.12 μmol of DOTAREM. An 80-mg aliquot of this mixture was hyperpolarized using a 3.35 T HyperSense (Oxford Instruments, Abingdon, UK) at a temperature of ~1.2 K using microwaves with a frequency of 94.115 GHz and power of 50 mW for up to ~1.5 h until visible (on the controlling computer screen) saturation of the polarization level. Under computer control, the sample underwent rapid dissolution in 6 mL of a solution containing 40 mM phosphate, 50 mM sodium chloride, and 40 mM sodium hydroxide (pH 7.4 at 10 bar and 180˚C) to give a final fumarate concentration of 39 mM, at pH 7.2.

RBC preparation

RBCs were obtained by cubital fossa venipuncture from a healthy donor (one of the investigators; Human Ethics cleared at all sites) and washing in iso-osmotic phosphate-buffered saline (PBS; 286 mOsm kg^{-1}, pH 7.25). Collected blood was centrifuged (10 min, 3000*g*, 4˚C) and the supernatant and buffy coat were aspirated and discarded. The process of re-suspension of the cells in PBS, centrifugation and supernatant aspiration was repeated twice. For the ^{1}H-NMR experiments, the suspensions were bubbled with carbon monoxide for 10 min before the final wash. This was done in order to stabilize hemoglobin inside RBCs in a diamagnetic Fe(II) form (carboxyhemoglobin) for optimal spectral resolution and signal-to-noise ratio (S/N). After the final aspiration of the supernatant, the volume fraction of cells in the sample (hematocrit; *Ht*) was estimated and used in subsequent calculations; it was typically 80-87%. In experiments with hemolysates, RBC suspensions were subjected to two cycles of freezing in liquid nitrogen and thawing at ~30˚C. The samples were used for NMR measurements on the same day.

NMR spectroscopy

^{1}H-NMR spectra were recorded at 400.13 MHz on a Bruker (Karlsruhe, Germany) Avance III console with a 9.4 T vertical wide-bore magnet from Oxford Instruments (Oxford, UK), equipped with a 10-mm Bruker broadband (BBO) probe.

2.0 mL of freshly prepared hemolysate was added to a 10-mm NMR tube and thermally pre-equilibrated at 37˚C inside the spectrometer bore. Then, 1.0-2.0 mL of sodium fumarate solution in PBS (pH 7.2) was injected rapidly via a heat-exchanging system designed to pre-equilibrate the fumarate solution to 37˚C, with subsequent mixing.[21]

Monitoring the fumarase reaction by recording sequential NMR spectra was started at the time of the injection. Single-transient ^{1}H spin-echo NMR spectra[18] were acquired every 5 s over a duration of ~20 min using a 90˚ pulse of 29 μs, spectral width of 4 kHz, 4096 complex points, acquisition time of 1.024 s, and spin-echo delay τ = 291 ms, which corresponded to a total echo duration of 582 ms. In the experiments with the whole RBCs, the spin-echo delay was shortened to 190 ms. ^{13}C-NMR spectra were recorded on a Bruker Avance II 600 MHz spectrometer (150.9 MHz for ^{13}C) with a 14.1 T vertical magnet using a 10-mm Bruker broadband probe. The ^{13}C-NMR RD-DNP experiments involved injecting 2.0 mL of hyperpolarized [1,4-^{13}C]fumarate solution via the 37˚C heat-exchanger into a 10-mm NMR tube in the probe of the NMR spectrometer. The sample tube contained 2.0 mL of hemolysate that had been thermally equilibrated at 37˚C.

Data processing and analysis

All NMR spectra were processed using TopSpin 3.5 (Bruker); they were extracted as text files and read into *Mathematica*[22] programs. The spectra were phase corrected and baseline adjusted prior to analysis; exponential window functions with line broadening factors of 5.0 Hz and 10.0 Hz were used in the processing of ^{1}H and ^{13}C spectra, respectively. In some instances, several initial spectra showed inconsistent intensities due to incomplete sample mixing so they were discarded from the analysis.

The following kinetic modeling was based on the reaction time courses (temporal evolution of the fumarate and malate signals), which were processed by measuring the integrals of the corresponding peaks in each of the spectra, and then converting these values into respective concentrations, as described below.

In ^{1}H-NMR time courses, the single fumarate peak and the negative sum of the two malate peak integrals ($3H_R$ and $3H_S$) were used for the concentration calculations. Due to the phase modulation brought about by ^{1}H-^{1}H *J*-couplings, the ratio of the intensities of the fumarate and malate resonances did not reflect the correct ratio of their concentrations. Therefore, the latter values of fumarate and malate were obtained by deriving the two coefficients of proportionality between the measured integrals and the concentrations. These coefficients were obtained by a least-squared fit that optimized the condition of the sum of the two concentrations being as close as possible to the originally injected amount of fumarate (11.4 mM or 22.8 mM) for each point in the time course. Concentrations of endogenous fumarate and malate in blood are in the micromolar range,[23,24] thus

their contributions to the NMR signals were taken to be negligible. The obtained ^{1}H-NMR time course data were analyzed by regressing the numerical solution of the Michaelis-Menten equations in *Mathematica* using the function NonlinearModelFit.

In ^{13}C-NMR experiments, single-transient pulse-and-acquire spectra were obtained every 1 s for 256 s, using a small (~4˚) flip-angle pulse, spectral width of 40.65 kHz, 32768 complex points, and acquisition time of 0.806 s. Time courses of the ^{13}C-NMR signal intensities were constructed from the corresponding peak integrals. Only hyperpolarized NMR signals from fumarate and malate (Fum* and Mal*; see below) are observable in these spectra. Thus, the concentration of hyperpolarized fumarate [Fum*] was calculated for each point in the time course by assuming that the initial value of the curve, fitted to the peak-integral data, corresponded to the initial total concentration of fumarate that was known from the sample preparation. For calculation of the concentration of the hyperpolarized malate [Mal*], the integrals of the two peaks, corresponding to the inequivalent positions C1 and C4, were summed and these integral values were scaled by the same factor as those of fumarate.

The ^{13}C-NMR RD-DNP data were studied using FmR_{α} analysis to obtain initial estimates of the kinetic and relaxation rate constants. Next, the obtained estimates were used as starting parameter values in an MCMC method for fitting the mathematical representation of the fumarase reaction (see below). The application of a small flip-angle excitation pulse was built into the model to account for losses of signals due to the readout of the magnetizations at each time step. Our implementation of the MCMC algorithm was previously described in detail.[20,25,26].

RESULTS

^{1}H NMR of hemolysates

Figure 1 shows a stacked plot of typical ^{1}H spin-echo NMR spectra obtained upon addition of fumarate to a hemolysate, along with the corresponding spectral assignments. Fumarate injection resulted in the immediate appearance of a singlet at 6.49 ppm, corresponding to the two equivalent hydrogen atoms of fumarate (2H and 3H). Subsequently, the conversion of fumarate into malate was evidenced by the decline of the fumarate signal and appearance of three peaks, corresponding to the three inequivalent hydrogen atoms of malate: 2H (4.27 ppm), $3H_R$ (2.64 ppm) and $3H_S$ (2.33 ppm). The peaks corresponding to $3H_R$ and $3H_S$ had negative intensities due to the ^{1}H-^{1}H *J*-coupling modulations for the chosen value of the delay τ (291 ms) in the spin-echo experiment.

The peak at 1.30 ppm was assigned to 3H of lactate, which is present due to the ongoing glycolytic pathway from endogenous 2,3-biphosphoglycerate (23BPG). No other metabolites were seen in the spectra.

Figure 2 shows resultant time courses obtained upon injection of fumarate into hemolysates (for two final concentrations of fumarate: 22.8 or 11.4 mM). In the case of 11.4 mM fumarate, the equilibrium was reached after ~500 s (the curves reached a plateau), while it took approximately twice as long for equilibration when the amount of injected fumarate was doubled (22.8 mM). From the two time courses of Figure 2, the equilibrium constant $K_{\mathrm{eq}} = \frac{[\mathrm{Mal}]_{\mathrm{eq}}}{[\mathrm{Fum}]_{\mathrm{eq}}}$ was estimated to be 2.4 ± 0.1, where $[\mathrm{Mal}]_{\mathrm{eq}}$ and $[\mathrm{Fum}]_{\mathrm{eq}}$ are the equilibrium molar concentrations of malate and fumarate, respectively.

In the case of 22.8 mM fumarate, the initial part of the time course (first ~36 transients) was linear, which indicated full saturation of the enzyme at this high substrate concentration; in other words, this resulted in pseudo zero-order kinetics due to the near-constant reactant concentrations (fumarate and water). Fitting a straight line through the initial linear part of the time course allowed us to calculate the rate of fumarate conversion: 2.0 ± 0.1 mM min^{-1}, which corresponded to 4.6 ± 0.3 mmol (L RBC)$^{-1}$ min^{-1} when normalized by the volume of cells in the sample. This implied that a significant fraction of the ~10-20 mM hyperpolarized [1,4-^{13}C]fumarate, injected into a concentrated hemolysate, would be converted to L-malate in the ~3 min available in an ^{13}C-NMR RD-DNP experiment.

Modeling of ^{1}H-NMR time courses

Kinetic modeling of the experimental ^{1}H spin-echo time courses was based on the steady-state (with respect to the concentration of the enzyme-substrate complex) Michaelis-Menten equations, modified to account for competition between fumarate and malate for the active site in the enzyme. The concentration of the enzyme-substrate complex reaches a steady state within milliseconds for most enzymes,[27] so the Michaelis-Menten model remains fully valid (even in the case of RD-DNP analysis – see below). The differential equations that describe the kinetics of the reversible reaction of Equation 1 are:

$$\frac{d[\mathrm{Fum}]}{dt} = -k_1[\mathrm{Fum}] + k_{-1}[\mathrm{Mal}] \qquad (2)$$

$$\frac{d[\mathrm{Mal}]}{dt} = -k_{-1}[\mathrm{Mal}] + k_1[\mathrm{Fum}] \quad (3)$$

where [Fum] and [Mal] denote current (at a given time) molar concentrations of fumarate and malate, and the apparent unidirectional rate constants k_1 and k_{-1} apply to the forward and reverse reactions of Equation 1, respectively. According to the Michaelis-Menten model taking into account product inhibition,[28] these rate constants are, in turn, functions of the concentrations of fumarate and malate:

$$k_1 = \frac{V_{\mathrm{max}}^{\mathrm{Fum}}}{K_{\mathrm{m}}^{\mathrm{Fum}}\left(1+\frac{[\mathrm{Mal}]}{K_{\mathrm{m}}^{\mathrm{Mal}}}\right)+[\mathrm{Fum}]} \quad (4)$$

$$k_{-1} = \frac{V_{\mathrm{max}}^{\mathrm{Mal}}}{K_{\mathrm{m}}^{\mathrm{Mal}}\left(1+\frac{[\mathrm{Fum}]}{K_{\mathrm{m}}^{\mathrm{Fum}}}\right)+[\mathrm{Mal}]} \quad (5)$$

Where $V_{\mathrm{max}}^{\mathrm{Fum}}$ and $V_{\mathrm{max}}^{\mathrm{Mal}}$ are the maximum velocities of the forward and reverse reactions of Equation 1, respectively; $K_{\mathrm{m}}^{\mathrm{Fum}}$ and $K_{\mathrm{m}}^{\mathrm{Mal}}$ are the respective Michaelis constants of fumarase for fumarate and malate.

After the expressions of Equations 4-5 were substituted into Equations 2-3, the differential equations were solved numerically in *Mathematica*. The solutions of these equations were regressed onto the two experimental time courses of Figure 2 to estimate the values of the Michaelis-Menten parameters and the equilibrium constant K_{eq}, which, in turn, bears the following fundamental relationship with the Michelis-Menten parameters:[8]

$$K_{\mathrm{eq}} = \frac{[\mathrm{Mal}]_{\mathrm{eq}}}{[\mathrm{Fum}]_{\mathrm{eq}}} = \frac{K_{\mathrm{m}}^{\mathrm{Mal}}\, V_{\mathrm{max}}^{\mathrm{Fum}}}{K_{\mathrm{m}}^{\mathrm{Fum}}\, V_{\mathrm{max}}^{\mathrm{Mal}}} \quad (6)$$

In preliminary trial fits, it became evident that we could obtain equally good fits with various K_{m} values below ~1 mM. This implied the Michaelis constants of fumarase for fumarate and malate were in the micromolar range and, as the substrate concentrations used were all above 1 mM, the enzyme was effectively fully saturated at any time point in the reaction. Since the inherently low sensitivity of NMR spectroscopy would not allow measurements with substrate concentrations below 1 mM, we did not have the requisite information in the fitting curves to allow us to predict

reliably the K_m values in the micromolar range. Nevertheless, we proceeded with fitting of the available data by setting the starting values of K_m^{Fum} and K_m^{Mal} to 5.0 and 25.0 μM, respectively, as reported by Teipel et al.[10] The simultaneous fit of the two time-courses shown in Figure 2 yielded the following estimates of the Michaelis-Menten parameters: V_{max}^{Fum} = 5.9 ± 0.3 mmol (L RBC)$^{-1}$ min^{-1}; V_{max}^{Mal} = 16.0 ± 0.6 mmol (L RBC)$^{-1}$ min^{-1}; K_m^{Fum} = 3.9 ± 0.3 μM; K_m^{Mal} = 25.6 ± 1.0 μM; and K_{eq} = 2.4 ± 0.3, calculated using Equation 6.

^{1}H NMR of whole RBCs

Additionally, we investigated the rate of the fumarase reaction upon addition of fumarate to *whole intact* red blood cells. These experiments were conducted in the same way as the experiments with the hemolysates: 2.0 mL of a fumarate solution was injected into 2.0 mL of RBC suspension. In contrast to the hemolysate experiments, there was no evidence of the appearance of the malate peaks in the initial 10 min after commencing acquisition of the ^{1}H spin-echo NMR spectra (Figure 3). This was concluded to be because fumarase was initially located only inside the cells, and, since fumarate penetrates the plasma membrane of RBCs very slowly,[12] there was only very limited access of the injected fumarate to fumarase and hence a lack of reaction.

Having demonstrated no fumarase activity in the time course with whole RBCs for ~10 min, we injected 1.0 mL of the surfactant, Triton X-100, into the reaction medium via the same heat-exchange system that provided vigorous mixing. After this event, the conversion of fumarate to malate became evident (Figure 3).

In comparison with a typical hemolysate experiment (Figure 1), the spectral S/N was much poorer when intact RBCs were present; this was due to endogenous magnetic field gradients that they induce.[29] In order to obtain better S/N in the initial spectra, when samples consisted mostly of whole cells, we used a shorter spin-echo delay (τ = 190 ms). As the cells were being lysed in the presence of the surfactant, the S/N grew significantly. Therefore, for clarity of Figure 3, the amplitude of the fumarate peak was adjusted to be the same in all shown spectra. Shortening the spin-echo delay τ resulted in an altered pattern of signs of the malate peak intensities (Figure 3), due to the different modulation of the resonances by ^{1}H-^{1}H *J*-couplings. It was clear that, upon lysis of RBCs by the surfactant, the production of malate was substantially faster than in whole cells.

This experiment modeled the in vivo situation of fumarase release during necrosis/hemolysis in tumors. Thus, when fumarate is used as the 'pathological-state detection substrate',[11] the appearance of the malate signal could be due to ruptured RBCs in tumor nodules, in addition to lysed cancer cells.

^{13}C-NMR RD-DNP time courses

Figure 4 shows a stacked plot consisting of sequential ^{13}C-NMR spectra, obtained after injecting 2.0 mL of hyperpolarized [1,4-^{13}C]fumarate solution into 2.0 mL of a hemolysate, leading to a final substrate concentration of 22.2 mM and Ht = 42.5%. Injection of the hyperpolarized fumarate resulted in a strong ^{13}C-NMR resonance at 176.1 ppm. The intensity rapidly declined with a concurrent rise-and-fall of the resonances from [1,4-^{13}C]malate, at 182.5 and 181.3 ppm (Figure 4). As illustrated in Figure 5, the intensity of the malate resonance reached a maximum at t_{max} = ~20 s and it was smaller by a factor of ~100 than the starting intensity of the fumarate resonance. Both resonances had declined into the noise ~120 s after the injection.

^{13}C-NMR RD-DNP - FmR_α analysis

Initially, time courses of ^{13}C-NMR RD-DNP spectra were analyzed using our recently developed FmR_α analysis.[19] Figure 5 shows the application of this method to the time course of ^{13}C-NMR signal intensities of fumarate and malate, obtained using the spectra of Figure 4. Estimates of T_1 and the kinetic constant k_1 were made as follows. The ratio of the peak amplitude of the product and substrate at time t_{max} (denoted by 'P_{max}' and '$S[t_{max}]$' in Figure 5, respectively), gave the value of β = 0.025 (noting that the intensity of the product was scaled up by a factor of 20). FmR_α is the time-span of the horizontal line (green arrow) drawn at height α (88% of the maximum amplitude of the product's rise-and-fall curve).[19] According to the theory, this time corresponds to the average T_1 value of the two reactants; it was estimated to be ~18 s. The estimate of the apparent first-order rate constant k_1 that characterizes the reaction kinetics is given by $\beta/T_1 = \sim 1.4 \times 10^{-3}$ s^{-1}. Therefore, the initial reaction velocity, calculated as the value of k_1 multiplied by the initial fumarate concentration (and normalized to Ht = 100%) was 22.2 mM × 1.4 × 10^{-3} s^{-1} / 0.425 = 0.073 mmol (L RBC)$^{-1}$ s^{-1} or ~4.4 mmol (L RBC)$^{-1}$ min^{-1}. This value is in a very good agreement with the value of the initial flux of the reaction calculated by using ^{1}H-NMR time courses (see above).

^{13}C-NMR RD-DNP - MCMC analysis

Using the values of the kinetic and relaxation rate constants obtained via the *FmR$_\alpha$* analysis as the initial estimates, a more comprehensive kinetic characterization of the reaction was implemented using MCMC fitting of the Michaelis-Menten model to the experimental ^{13}C-NMR time courses. The model was based on a set of four coupled linear differential equations that describe the time evolution of the concentrations of the ^{13}C-labeled reactants involved in the reaction. As described previously,[21,30,31] each molecular species undergoing physical/chemical transformations in the RD-DNP experiments, might be conceptually split into two pools: hyperpolarized (or 'labeled') and non-hyperpolarized, with only the hyperpolarized species contributing to the detectable signal. The relevant kinetic scheme, which forms the basis for formulating the following kinetic equations, is shown in Figure 6; it leads to a system of four coupled differential equations:

$$\frac{d[\mathrm{Fum}^*]}{dt} = -\frac{1}{T_1^{\mathrm{Fum}}}[\mathrm{Fum}^*] - k_1[\mathrm{Fum}^*] + k_{-1}[\mathrm{Mal}^*] \quad (7)$$

$$\frac{d[\mathrm{Fum}]}{dt} = \frac{1}{T_1^{\mathrm{Fum}}}[\mathrm{Fum}^*] - k_1[\mathrm{Fum}] + k_{-1}[\mathrm{Mal}] \quad (8)$$

$$\frac{d[\mathrm{Mal}^*]}{dt} = -\frac{1}{T_1^{\mathrm{Mal}}}[\mathrm{Mal}^*] - k_{-1}[\mathrm{Mal}^*] + k_1[\mathrm{Fum}^*] \quad (9)$$

$$\frac{d[\mathrm{Mal}]}{dt} = \frac{1}{T_1^{\mathrm{Mal}}}[\mathrm{Mal}^*] - k_{-1}[\mathrm{Mal}] + k_1[\mathrm{Fum}] \quad (10)$$

where the asterisks denote the hyperpolarized species. The values of T_1 apply to fumarate (Fum) and malate (Mal), and the apparent unidirectional rate constants k_1 and k_{-1} characterize the flux in the forward and reverse reactions, as shown in Equation 1. While these equations are the basis of the *FmR$_\alpha$* analysis, they disregard the Michaelis-Menten nature of the kinetic processes; and it transpired that they did not lead to good fits to the experimental data shown in Figure 7A. Hence, the differential equations were further expanded to account for the effects of product inhibition/competition (see below), which allowed us to obtain a more comprehensive and statistically robust fit of the model to the experimental data.

According to the Michaelis-Menten model, the apparent unidirectional rate constants in Equations 7-10 can be expressed in terms of concentrations of the two competing substrates; however, a subtle point worth noting is that these concentrations must contain the sums of both hyperpolarized and non-hyperpolarized species:

$$k_1 = \frac{V_{\max}^{\mathrm{Fum}}}{K_{\mathrm{m}}^{\mathrm{Fum}}\left(1+\frac{[\mathrm{Mal}]+[\mathrm{Mal}^*]}{K_{\mathrm{m}}^{\mathrm{Mal}}}\right)+[\mathrm{Fum}]+[\mathrm{Fum}^*]} \tag{11}$$

$$k_{-1} = \frac{V_{\max}^{\mathrm{Mal}}}{K_{\mathrm{m}}^{\mathrm{Mal}}\left(1+\frac{[\mathrm{Fum}]+[\mathrm{Fum}^*]}{K_{\mathrm{m}}^{\mathrm{Fum}}}\right)+[\mathrm{Mal}]+[\mathrm{Mal}^*]} \tag{12}$$

where, as before, the asterisks denote the hyperpolarized species; the maximal velocities $V_{\max}^{\mathrm{Fum}}$ and $V_{\max}^{\mathrm{Mal}}$ apply to the forward (Fum) and reverse (Mal) reactions of Equation 1, respectively, as do the respective Michaelis constants $K_{\mathrm{m}}^{\mathrm{Fum}}$ and $K_{\mathrm{m}}^{\mathrm{Mal}}$.

Substitution of Equations 11-12 into Equations 7-10 allows us to obtain a set of differential equations that accounts for the reaction kinetics with the possibility of enzyme saturation and variable kinetic order that depends on reactant concentration:

$$\frac{d[\mathrm{Fum}^*]}{dt} = -\frac{[\mathrm{Fum}^*]}{T_1^{\mathrm{Fum}}} - \frac{V_{\max}^{\mathrm{Fum}}[\mathrm{Fum}^*]}{K_{\mathrm{m}}^{\mathrm{Fum}}\left(1+\frac{[\mathrm{Mal}]+[\mathrm{Mal}^*]}{K_{\mathrm{m}}^{\mathrm{Mal}}}\right)+[\mathrm{Fum}]+[\mathrm{Fum}^*]} + \frac{V_{\max}^{\mathrm{Mal}}[\mathrm{Mal}^*]}{K_{\mathrm{m}}^{\mathrm{Mal}}\left(1+\frac{[\mathrm{Fum}]+[\mathrm{Fum}^*]}{K_{\mathrm{m}}^{\mathrm{Fum}}}\right)+[\mathrm{Mal}]+[\mathrm{Mal}^*]} \tag{13}$$

$$\frac{d[\mathrm{Fum}]}{dt} = \frac{[\mathrm{Fum}^*]}{T_1^{\mathrm{Fum}}} - \frac{V_{\max}^{\mathrm{Fum}}[\mathrm{Fum}]}{K_{\mathrm{m}}^{\mathrm{Fum}}\left(1+\frac{[\mathrm{Mal}]+[\mathrm{Mal}^*]}{K_{\mathrm{m}}^{\mathrm{Mal}}}\right)+[\mathrm{Fum}]+[\mathrm{Fum}^*]} + \frac{V_{\max}^{\mathrm{Mal}}[\mathrm{Mal}]}{K_{\mathrm{m}}^{\mathrm{Mal}}\left(1+\frac{[\mathrm{Fum}]+[\mathrm{Fum}^*]}{K_{\mathrm{m}}^{\mathrm{Fum}}}\right)+[\mathrm{Mal}]+[\mathrm{Mal}^*]} \tag{14}$$

$$\frac{d[\mathrm{Mal}^*]}{dt} = -\frac{[\mathrm{Mal}^*]}{T_1^{\mathrm{Mal}}} - \frac{V_{\max}^{\mathrm{Mal}}[\mathrm{Mal}^*]}{K_{\mathrm{m}}^{\mathrm{Mal}}\left(1+\frac{[\mathrm{Fum}]+[\mathrm{Fum}^*]}{K_{\mathrm{m}}^{\mathrm{Fum}}}\right)+[\mathrm{Mal}]+[\mathrm{Mal}^*]} + \frac{V_{\max}^{\mathrm{Fum}}[\mathrm{Fum}^*]}{K_{\mathrm{m}}^{\mathrm{Fum}}\left(1+\frac{[\mathrm{Mal}]+[\mathrm{Mal}^*]}{K_{\mathrm{m}}^{\mathrm{Mal}}}\right)+[\mathrm{Fum}]+[\mathrm{Fum}^*]} \tag{15}$$

$$\frac{d[\mathrm{Mal}]}{dt} = \frac{[\mathrm{Mal}^*]}{T_1^{\mathrm{Mal}}} - \frac{V_{\max}^{\mathrm{Mal}}[\mathrm{Mal}]}{K_{\mathrm{m}}^{\mathrm{Mal}}\left(1+\frac{[\mathrm{Fum}]+[\mathrm{Fum}^*]}{K_{\mathrm{m}}^{\mathrm{Fum}}}\right)+[\mathrm{Mal}]+[\mathrm{Mal}^*]} + \frac{V_{\max}^{\mathrm{Fum}}[\mathrm{Fum}]}{K_{\mathrm{m}}^{\mathrm{Fum}}\left(1+\frac{[\mathrm{Mal}]+[\mathrm{Mal}^*]}{K_{\mathrm{m}}^{\mathrm{Mal}}}\right)+[\mathrm{Fum}]+[\mathrm{Fum}^*]} \tag{16}$$

Thus, the numerical solutions of Equations 13-16 were fitted using the MCMC algorithm to the experimental ^{13}C-NMR time courses. The MCMC analysis performed well in terms of generating reproducible estimates of the fitted parameters, once the parameter space had been restricted by

fixing the values of α (the flip-angle of the magnetization-sampling radiofrequency pulse) to 4°, and previously determined equilibrium constant K_{eq} to 2.4. Thus, only the maximal velocities, Michaelis constants, T_1 values and the initial concentration of the hyperpolarized fumarate [Fum*](0) were floated. Fitting systematically gave values of the order of 1 mM for K_m^{Fum} and K_m^{Mal}. Since the reaction was studied at supra-physiological substrate concentrations, the enzyme would be expected to be fully saturated for the whole time over which the reaction was able to be monitored. This meant that the values of the Michaelis constants could not be reliably estimated. Thus, the value of K_m^{Fum} was fixed at 3.9 μM (value, obtained from fitting of the ^{1}H-NMR data), while the value of K_m^{Mal} was automatically calculated at each time step using Equation 6.
Figure 7A shows an MCMC fit to the data obtained using the time-course data of Figure 5. The robustness of the MCMC fits in the context of modeling the fumarase reaction was assessed using a statistical 'sensitivity analysis'.[32] This entailed random variation of the parameter values, and accepting only those changes to the 'parameter chain' that led to a deacrease or an insignificant increase in the fit score (calculated as the root mean square deviation (RMSD) between the experimental and simulated time-course curves). The process of the variation of the parameter values was repeated for 20,000 iterations and the RMSD criterion was adjusted so that the acceptance rate was ~35%. This procedure allowed us to generate arrays of numerical values for each of the fitted parameters, which were used to visualize their dispersions, as shown in Figure 7B for T_1^{Fum}, T_1^{Mal}, V_{max}^{Fum} and [Fum*](0). Based on the obtained near-Gaussian distributions (Figure 7B), the means and standard deviations for each of the parameters were calculated. The analysis resulted in the following estimated values of parameters (after constraining $\alpha = 4^o$, $K_{eq} = 2.4$, $K_m^{Fum} = 3.9$ μM): $T_1^{Fum} = 20.7 \pm 0.5$ s; $T_1^{Mal} = 19.1 \pm 3.4$ s; V_{max}^{Fum} = 4.0 ± 0.8 mmol (L RBC)$^{-1}$ min^{-1}; V_{max}^{Mal} = 13.0 ± 4.7 mmol (L RBC)$^{-1}$ min^{-1}; and initial concentration of [Fum*](0) = 20.9 ± 0.3 mM.

DISCUSSION

^{1}H-NMR time courses

The ^{1}H-NMR time courses (Figure 2) showed that the rate of the fumarate-to-malate conversion in hemolysates was close to that reported by Simpson et al.[12] In this previous work, the half-life of conversion of 30 mM fumarate (in a hemolysate of *Ht* = 83%) was ~3 min. A detailed kinetic characterization of RBC fumarase was not the aim of that work; nevertheless, the maximum flux

measured in our work (4.6 ± 0.3 mmol (L RBC)$^{-1}$ min^{-1}) corresponded to conversion of 11.5 mM of fumarate in 3 min in a hemolysate of *Ht* = 83%, while it would have implied conversion of 15 mM fumarate using the previously reported rate.[12] The experimental conditions differed in both projects, especially the freshness of the hemolysates, so a comparison must be made cautiously. Nevertheless, estimating a reaction rate to within a factor of ~1.5 of the previous work was encouraging for the next series of measurements. Importantly, the rates estimated from the ^{1}H-NMR experiments indicated that the fumarase reaction in hemolysates was sufficiently rapid to be characterized successfully by the ^{13}C-NMR RD-DNP experiments, the latter being especially useful for the kinetic characterization of metabolic processes in vivo.

Theoretically, malate can be further converted in RBCs to oxaloacetate, pyruvate and lactate.[12] This pathway occurs via oxidation of malate by malate dehydrogenase (EC 1.1.1.37) and requires significant levels of free NAD^+/NADH in the system. However, in hemolysates most of the free NAD^+/NADH is destroyed by contact with the $NAD(P)^+$ nucleosidase (EC 3.2.2.6) which is located on the cell exterior.[33] Thus, the rate of malate to lactate conversion in hemolysates was reported to be negligible when no external NAD^+ is added to the sample,[12] and we concluded that the lactate seen in our spectra (Figure 1) was produced via glycolysis from 23BPG.

The equilibrium constant of the fumarase reaction (K_{eq}) was previously shown to be a function of the ionic strength of the medium, temperature, and pH.[8,34] Bock and Alberty reported K_{eq} = ~4.8 at an ionic strength of 0.50 M, pH 7.3 and 25˚C, while Scott and Powell reported K_{eq} = 3.8 under the same buffer conditions.[34] Our value of K_{eq} = 2.4 is closer to the value of 3.1, reported by Borsook and Schott,[35] while the Michaelis constant of fumarase for fumarate (3.9 ± 0.3 μM) and malate (25.6 ± 1.0 μM) are in agreement with the literature values.[10]

^{13}C-NMR RD-DNP time courses

The observed decay of the ^{13}C-NMR RD-DNP fumarate signal and the concurrent rise-and-fall of that of malate were conveniently suitable for the application of the FmR_α analysis.[19] The initial velocity of the reaction, computed using this procedure (4.4 mmol (L RBC)$^{-1}$ min^{-1}), was very similar to that estimated from our ^{1}H-NMR data (4.6 ± 0.3 mmol (L RBC)$^{-1}$ min^{-1}). Note that this rate is ~150 times faster than RBC glycolysis,[1] so fumarase activity in human RBCs is indeed very high in comparison with the 'housekeeping' carbon flux.

The four first-order differential equations (Equations 13-16) constitute a minimalist model of fumarase as a reversible Michaelis-Menten enzyme. The magnetization-relaxation part of these equations (formally called the Bloch-McConnell equations) is represented by first-order decay terms, characterized by the relaxation time constants (T_1), while the chemical exchange parts are derived from the steady-state Michaelis-Menten equation. An important subtlety in formulating these chemical-exchange equations is that the denominators in the expressions for rate constants must contain the sums of the concentrations of all of the relevant species, whether hyperpolarized or not, because it is the total chemical potential of the species that drives the chemical exchange reaction (mediated by fumarase in this case).

The Michaelis constants of fumarase are known to be in the micromolar range,[10] but the inherently low sensitivity of the NMR techniques requires the use of substrate concentrations at least in the millimolar range. This meant that the kinetics of the fumarase reaction was virtually zero-order upon the initial injection of fumarate. However, as the product of the reaction (malate) was being accumulated, the reaction was increasingly subjected to product inhibition, according to the ratio of the two Michaelis constants and maximum velocities.

Estimated maximum velocities of the reaction in the forward and reverse direction were found to be 4.0 ± 0.8 and 13.0 ± 4.7 mmol (L RBC)$^{-1}$ min^{-1}, respectively; these values were slightly lower that the corresponding estimates from the ^{1}H-NMR measurements: 5.9 ± 0.3 and 16.0 ± 0.6 mmol (L RBC)$^{-1}$ min^{-1}. Since the donor for each of the experiments was the same person, biological variability was not the basis of this finding. Additionally, the stability of the linewidth and chemical shifts of all the peaks in both ^{1}H- and ^{13}C-NMR time course data indicated that the temperature was well-equilibrated across the sample before the acquisition of the NMR data began. Therefore, we concluded that variability in the estimates of the kinetic parameters between the ^{1}H and ^{13}C-NMR data was not caused by gradients in the sample temperature.

Nevertheless, there were some differences in the chemical composition of the media between the ^{1}H and ^{13}C-NMR experiments, which were unavoidable due to the specific requirements for the preparation of the hyperpolarized samples. Specifically, the trityl radical DOTAREM and solvent DMSO were present in the samples for the RD-DNP experiments. Although the final concentrations of these compounds were small, we cannot rule out the possibility of them having an effect on the fumarase reaction. Phosphate, on the other hand, is a known effector of fumarase (activating reagent). After the volume of the sample occupied by the cells was taken into account,

the final concentration of phosphate in the NMR sample, in the ^{1}H spin-echo and ^{13}C RD-DNP experiments, was 5.75 and 20.75 mM, respectively. According to Table 1 of Massey,[36] the relative activity of fumarase at pH 7.4 in the former case would be ~54 activity units, compared with ~56 activity units in the latter. Thus, the effect of our particular phosphate concentration was deemed to be non-significant (~3-4% variation) and would not fully account for the observed difference in the fumarase activity.

The estimates of T_1 values were in good agreement among the two methods used to obtain them: ~18 s (FmR_a); T_1^{Fum} = 20.7 ± 0.5 s and T_1^{Mal} = 19.1 ± 3.4 s (MCMC). These values also corresponded well to those previously obtained by Gallagher et al.[11] using a similar methodology to ours: T_1^{Fum} = 24.1 ± 2.1 s and T_1^{Mal} = 18.4 ± 7.0 s.

Implications for in vivo studies

While our ^{1}H-NMR study demonstrated that the equilibration of the fumarase reaction occurred over a time domain of ~20 min (after initial injection of 22.8 mM fumarate), the counterpart ^{13}C-NMR RD-DNP experiment allowed us to monitor the reaction only for the initial ~100 s after injection. Thus, an extent of the fumarase reaction only up to ~8-10% was able to be monitored in the latter experiment. It is the rapid decay of the nuclear polarization (according to the T_1 values of metabolites) that limits the time domain over which the ^{13}C RD-DNP technique is applicable.

Gallagher et al.[11] reported k_1 = 0.018 s^{-1} in drug-treated tumors. Assuming that there was ~10% of blood by volume, *Ht* of ~50%, and the tumor size was ~2 cm^3,[37] there would be ~10^{-4} L of RBCs in the tumor. According to the estimates of $V_{\mathrm{max}}^{\mathrm{Fum}}$ reported here, in the case of 100% hemolysis, this would correspond to maximum reaction flux of 0.03 mmol s^{-1} in the forward direction. Given that the amount of injected fumarate was 3.23 mmol,[11] the reaction rate constant k_1 due the RBC fumarase could be as high as 0.009 s^{-1}, or half of the rate constant observed in tumor-bearing mice.[11]

Thus, we deduce that the capacity of the fumarase-catalyzed reaction in RBCs is so high that hemolysed RBCs could contribute significantly to the overall metabolism of [1,4-^{13}C]fumarate in necrotic tumors in vivo. As a proof-of-principle, this was demonstrated using the experiment with a detergent that lysed the RBCs and released fumarase into the extracellular medium (Figure 3).

Even though neoplastic formation is not typically associated with hemolysis, there are at least three factors which might mediate the rupture of RBCs in a tumor: autoimmune processes (autoimmune

hemolytic anemia),[38] microangiopathic disorders[38-41] and chemotherapy.[38,42,43] The deduction about the contribution of ruptured RBCs to the fumarase reaction in necrotic tissues awaits verification, by making measurements on tumor tissue or cancer-cell suspensions in vitro. The NMR and data-analysis methodologies developed here will be beneficial for these future studies.

Conclusions and future directions

We conducted ^{1}H spin-echo and ^{13}C RD-DNP NMR studies of human red blood cell fumarase in hemolysates and whole cells using injections of exogenous fumarate. We demonstrated that, in both experiments, the kinetics of the fumarase reaction could be quantified by fitting a mathematical model to the reaction time course data. To our knowledge, a detailed in situ (in vitro) study of the RBC fumarase kinetics is reported here for the first time. The estimated rate of the reaction was in the range 4-6 mmol (L RBC)$^{-1}$ min^{-1}, which was sufficiently high to enable the kinetic characterization of the enzyme with ^{13}C-labeled fumarate in RD-DNP experiments. High fumarase activity in RBCs indicates a potential contribution of hemolysis to measurements of the extent of necrosis in tumors in vivo by using hyperpolarized fumarate. The experimental (NMR) and *Mathematica*-based procedures for data analysis developed here have them poised for applications to the kinetic characterization of other enzymes in cell lysates, whole cells, and tissues.

ACKNOWLEDGEMENTS

The work was funded by a Discovery Project Grant from the Australian Research Council to PWK (DP140102596), and a European Research Council (ERC) grant to GP. The Leverhulme Trust supported a Visiting Professorship for PWK in the Group of Professor Malcolm Levitt and GP in the School of Chemistry at the University of Southampton. Work in K.M. Brindle's laboratory is supported by a Cancer Research UK Programme grant (17242) and the CRUK-EPSRC Imaging Centre in Cambridge and Manchester (16465).

REFERENCES

1. Mulquiney PJ, Bubb WA, Kuchel PW. Model of 2,3-bisphosphoglycerate metabolism in the human erythrocyte based on detailed enzyme kinetic equations: in vivo kinetic characterization of 2,3-bisphosphoglycerate synthase/phosphatase using ^{13}C and ^{31}P NMR. Biochem J 1999;342:567-580.
2. Mulquiney PJ, Kuchel PW. Model of 2,3-bisphosphoglycerate metabolism in the human erythrocyte based on detailed enzyme kinetic equations: equations and parameter refinement. Biochem J 1999;342:581-596.
3. Mulquiney PJ, Kuchel PW. Model of 2,3-bisphosphoglycerate metabolism in the human erythrocyte based on detailed enzyme kinetic equations: computer simulation and metabolic control analysis. Biochem J 1999;342:597-604.
4. Kuchel PW, Mulquiney PJ. Combined NMR experimental and computer-simulation study of 2,3-bisphosphoglycerate metabolism in human erythrocytes. In: Cornish-Bowden A, Cárdenas ML, editors. Technological and medical implications of metabolic control analysis. Dordrecht: Springer Netherlands; 2000. p. 139-145.
5. Nelson SJ, Kurhanewicz J, Vigneron DB, Larson PEZ, Harzstark AL, Ferrone M, van Criekinge M, Chang JW, Bok R, Park I, Reed G, Carvajal L, Small EJ, Munster P, Weinberg VK, Ardenkjaer-Larsen JH, Chen AP, Hurd RE, Odegardstuen L-I, Robb FJ, Tropp J, Murray JA. Metabolic imaging of patients with prostate cancer using hyperpolarized [1-^{13}C]pyruvate. Sci Transl Med 2013;5:198ra108.
6. Ardenkjær-Larsen JH, Fridlund B, Gram A, Hansson G, Hansson L, Lerche MH, Servin R, Thaning M, Golman K. Increase in signal-to-noise ratio of >10,000 times in liquid-state NMR. Proc Natl Acad Sci U S A 2003;100:10158-10163.
7. Jensen PR, Karlsson M, Lerche MH, Meier S. Real-time DNP NMR observations of acetic acid uptake, intracellular acidification, and of consequences for glycolysis and alcoholic fermentation in yeast. Chem - Eur J 2013;19:13288-13293.
8. Bock RM, Alberty RA. Studies of the enzyme fumarase. I. Kinetics and equilibrium. J Am Chem Soc 1953;75:1921-1925.
9. Brant DA, Barnett LB, Alberty RA. The temperature dependence of the steady state kinetic parameters of the fumarase reaction. J Am Chem Soc 1963;85:2204-2209.
10. Teipel JW, Hass GM, Hill RL. The substrate specificity of fumarase. J Biol Chem 1968;243:5684-5694.
11. Gallagher FA, Kettunen MI, Hu D-E, Jensen PR, in 't Zandt R, Karlsson M, Gisselsson A, Nelson SK, Witney TH, Bohndiek SE, Hansson G, Peitersen T, Lerche MH, Brindle KM. Production of hyperpolarized [1,4-$^{13}C_2$]malate from [1,4-$^{13}C_2$]fumarate is a marker of cell necrosis and treatment response in tumors. Proc Natl Acad Sci U S A 2009;106:19801-19806.
12. Simpson RJ, Brindle KM, Campbell ID. Spin echo proton NMR studies of the metabolism of malate and fumarate in human erythrocytes: dependence on free NAD levels. Biochim Biophys Acta 1982;707:191-200.
13. Witney TH, Kettunen MI, Hu D-E, Gallagher FA, Bohndiek SE, Napolitano R, Brindle KM. Detecting treatment response in a model of human breast adenocarcinoma using hyperpolarised [1-^{13}C]pyruvate and [1,4-$^{13}C_2$]fumarate. Br J Cancer 2010;103:1400-1406.
14. Yogev O, Yogev O, Singer E, Shaulian E, Goldberg M, Fox TD, Pines O. Fumarase: a mitochondrial metabolic enzyme and a cytosolic/nuclear component of the DNA damage response. PLoS Biol 2010;8:e1000328.

15. Yogev O, Naamati A, Pines O. Fumarase: a paradigm of dual targeting and dual localized functions. FEBS J 2011;278:4230-4242.
16. Quastel JH. The action of dyestuffs on enzymes. II. Fumarase. Biochem J 1931;25:898-913.
17. Tanaka KR, Valentine WN. Fumarase activity of human leukocytes and erythrocytes. Blood 1961;17:328-333.
18. Brown FF, Campbell ID, Kuchel PW, Rabenstein DL. Human erythrocyte metabolism studies by ^{1}H spin echo NMR. FEBS Lett 1977;82:12-16.
19. Pagès G, Kuchel PW. FmR_{α} analysis: rapid and direct estimation of relaxation and kinetic parameters from dynamic nuclear polarization time courses. Magn Reson Med 2015;73:2075-2080.
20. Kuchel PW, Naumann C, Puckeridge M, Chapman BE, Szekely D. Relaxation times of spin states of all ranks and orders of quadrupolar nuclei estimated from NMR *z*-spectra: Markov chain Monte Carlo analysis applied to $^{7}Li^{+}$ and $^{23}Na^{+}$ in stretched hydrogels. J Magn Reson 2011;212:40-46.
21. Pagès G, Puckeridge M, Liangfeng G, Tan YL, Jacob C, Garland M, Kuchel PW. Transmembrane exchange of hyperpolarized ^{13}C-urea in human erythrocytes: subminute timescale kinetic analysis. Biophys J 2013;105:1956-1966.
22. Wolfram S. The Mathematica Book. 5th ed. Champaign: Wolfram Media; 2003. 1488 p.
23. Nordmann J, Nordmann R. Organic acids in blood and urine. Adv Clin Chem 1961;4:53-120.
24. Hummel JP. The fluorometric determination of malic acid. J Biol Chem 1949;180:1225-1228.
25. Puckeridge M, Chapman BE, Conigrave AD, Grieve SM, Figtree GA, Kuchel PW. Stoichiometric relationship between Na^{+} ions transported and glucose consumed in human erythrocytes: Bayesian analysis of ^{23}Na and ^{13}C NMR time course data. Biophys J 2013;104:1676-1684.
26. Shishmarev D, Chapman BE, Naumann C, Mamone S, Kuchel PW. ^{1}H NMR *z*-spectra of acetate methyl in stretched hydrogels: quantum-mechanical description and Markov chain Monte Carlo relaxation-parameter estimation. J Magn Reson 2015;250:29-36.
27. Nelson DL, Cox MM. Lehninger Principles of Biochemistry. 5th ed. New York: W.H. Freeman and Company; 2008. 1100 p.
28. Cornish-Bowden A. Fundamentals of enzyme kinetics. 4th ed. Weinheim: Wiley-Blackwell; 2012. 510 p.
29. Endre ZH, Kuchel PW, Chapman BE. Cell volume dependence of ^{1}H spin-echo NMR signals in human erythrocyte suspensions: the influence of in situ field gradients. Biochim Biophys Acta 1984;803:137-144.
30. Pagès G, Tan YL, Kuchel PW. Hyperpolarized [1,^{13}C]pyruvate in lysed human erythrocytes: effects of co-substrate supply on reaction time courses. NMR Biomed 2014;27:1203-1210.
31. Pagès G, Kuchel PW. Mathematical modeling and data analysis of NMR experiments using hyperpolarized ^{13}C metabolites. Magn Reson Insights 2013;6:13-21.
32. Bankson JA, Walker CM, Ramirez MS, Stefan W, Fuentes D, Merritt ME, Lee J, Sandulache VC, Chen Y, Phan L, Chou P-C, Rao A, Yeung S-CJ, Lee M-H, Schellingerhout D, Conrad CA, Malloy C, Sherry AD, Lai SY, Hazle JD. Kinetic modeling and constrained

reconstruction of hyperpolarized [1-^{13}C]-pyruvate offers improved metabolic imaging of tumors. Cancer Res 2015;75:4708-4717.
33. Simpson RJ, Brindle KM, Brown FF, Campbell ID, Foxall DL. Studies of lactate dehydrogenase in the purified state and in intact erythrocytes. Biochem J 1982;202:581-587.
34. Scott EM, Powell R. Kinetics of the fumarase system. J Am Chem Soc 1948;70:1104-1107.
35. Borsook H, Schott HF. The role of the enzyme in the succinate-enzyme-fumarate equilibrium. J Biol Chem 1931;92:535-557.
36. Massey V. Studies on fumarase. 2. The effects of inorganic anions on fumarase activity. Biochem J 1953;53:67-71.
37. Day SE, Kettunen MI, Gallagher FA, Hu D-E, Lerche M, Wolber J, Golman K, Ardenkjaer-Larsen JH, Brindle KM. Detecting tumor response to treatment using hyperpolarized ^{13}C magnetic resonance imaging and spectroscopy. Nat Med 2007;13:1382-1387.
38. Rytting M, Worth L, Jaffe N. Hemolytic disorders associated with cancer. Hematol/Oncol Clin 1996;10:365-376.
39. Lohrmann H-P, Adam W, Heymer B, Kubanek B. Microangiopathic hemolytic anemia in metastatic carcinoma: report of eight cases. Ann Intern Med 1973;79:368-375.
40. Lechner K, Obermeier HL. Cancer-related microangiopathic hemolytic anemia: clinical and laboratory features in 168 reported cases. Medicine 2012;91:195-205.
41. Antman KH, Skarin AT, Mayer RJ, Hargreaves HK, Canellos GP. Microangiopathic hemolytic anemia and cancer: a review. Medicine 1979;58:377-384.
42. Dumez H, Guetens G, De Boeck G, Highley MS, Maes RAA, van Oosterom AT, de Bruijn EA. The relevance of therapeutic drug monitoring in plasma and erythrocytes in anti-cancer drug treatment. Clin Chem Lab Med 2004;42:1219-1227.
43. Schauf B, Schweizer N, Solomayer E, Wallwiener D, Huober J. Direct toxic effect of cytostatic drugs on erythrocytes as possible reason for chemotherapy-induced anemia. J Clin Oncol 2004;22:781-781.

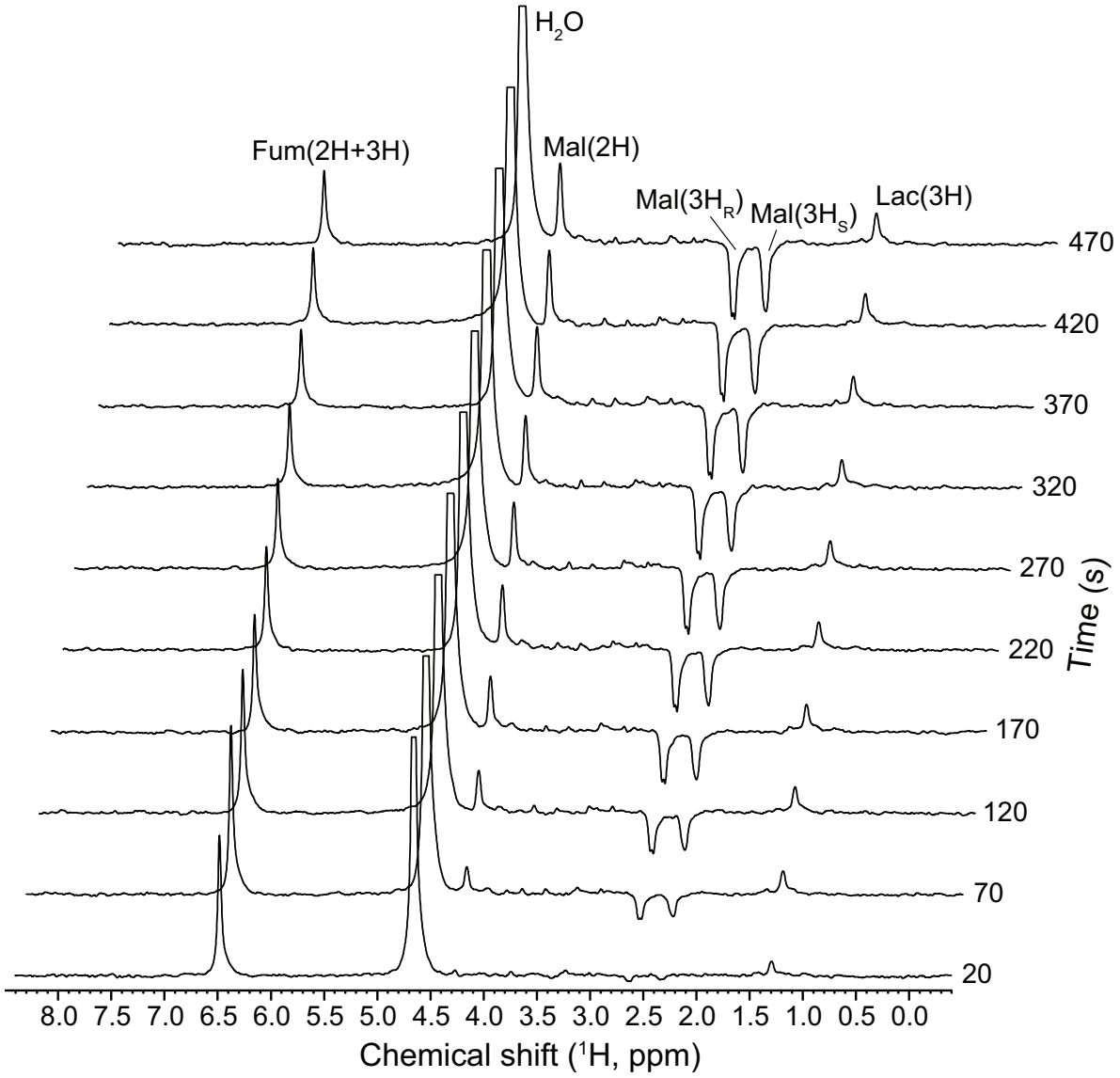

Figure 1. A representative time course of ^{1}H spin-echo NMR spectra of hemolysates. The spectra were acquired at 37˚C every 5 s over a period of ~10 min upon injection of a fumarate solution (final *Ht* = 43.5% and 11.4 mM fumarate). For clarity, only every tenth spectrum is shown. The signal from the fumarate is at 6.49 ppm; the signals from malate are at 2.33, 2.64 and 4.27 ppm; the resonance at 1.30 ppm was assigned to the methyl group of lactate.

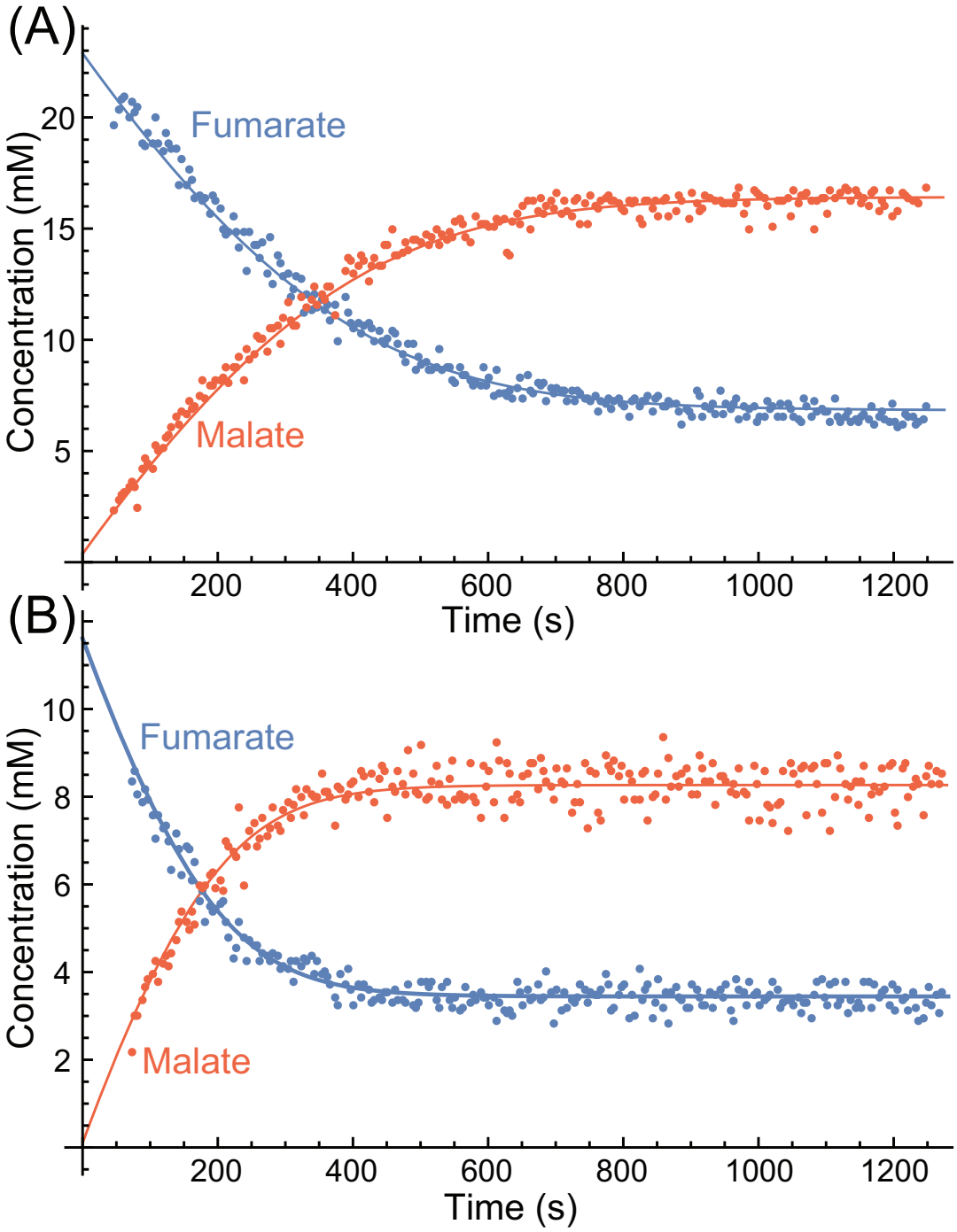

Figure 2. Fumarase activity in fresh hemolysates (*Ht* = 43.5%), recorded using ^{1}H spin-echo NMR spectra at 37˚C every 5 s over the course of ~20 min. Temporal evolution of the calculated concentrations of fumarate (blue dots) and malate (red dots) were plotted. The time courses were obtained by injection of (A) 22.8 mM and (B) 11.4 mM fumarate. Solid lines are nonlinear regression analysis fits of the Michaelis-Menten model. The estimated best-fit parameter value were: V_{max}^{Fum} = 5.9 ± 0.3 mmol (L RBC)$^{-1}$ min^{-1}; V_{max}^{Mal} = 16.0 ± 0.6 mmol (L RBC)$^{-1}$ min^{-1}; K_m^{Fum} = 3.9 ± 0.3 μM; K_m^{Mal} = 25.6 ± 1.0 μM; and K_{eq} = 2.4 ± 0.3.

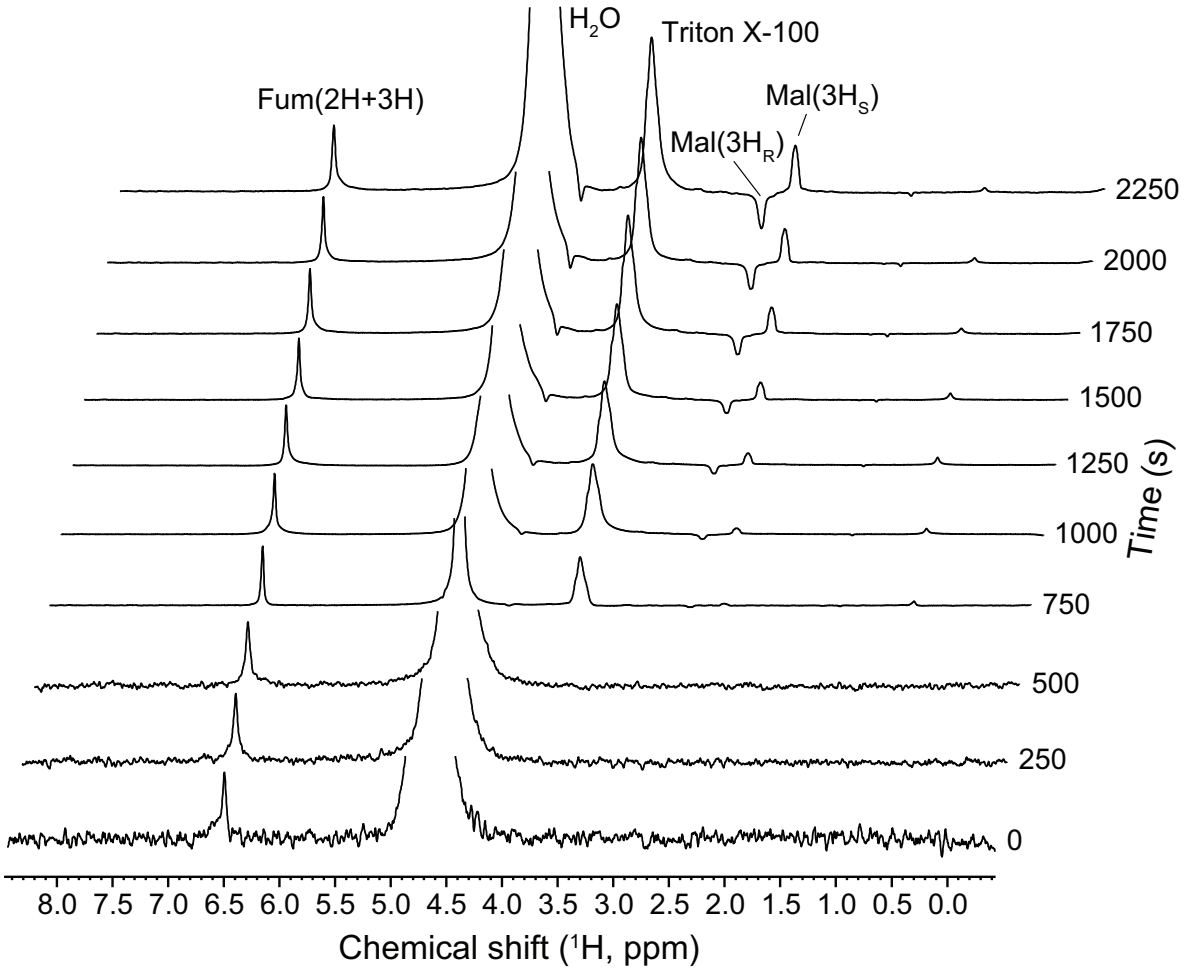

Figure 3. A fumarase-reaction time course of ^{1}H spin-echo NMR spectra in whole RBCs. The spectra were acquired at 37˚C every 5 s over a period of ~40 min upon injection of 2.0 mL of the fumarate solution into an RBC suspension (final *Ht* = 43.5% and 44.8 mM fumarate). After ~10 min from the start of the reaction, 1.0 mL of Triton X-100 was injected into the medium. The relevant peak assignments are indicated above the top spectrum. For clarity, every tenth spectrum is shown and the amplitude of the fumarate peak was adjusted to be the same in all shown spectra.

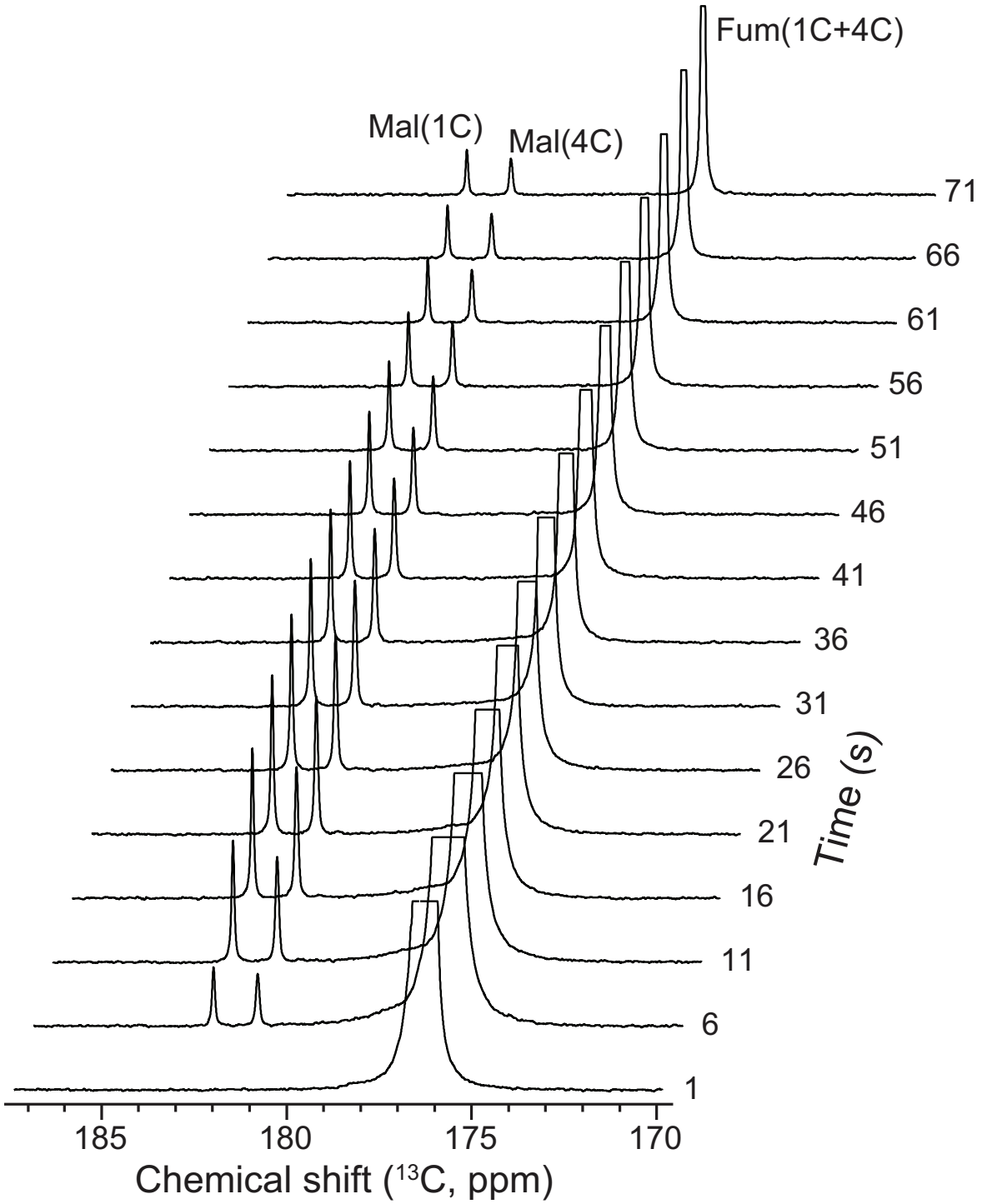

Figure 4. Representative ^{13}C-NMR spectra of hemolysates, acquired at 37˚C every 1 s over a period of 256 s, after injection of a hyperpolarized solution of [1,4-^{13}C]fumarate (final *Ht* = 42.5% and 22.2 mM fumarate). For clarity, every fifth spectrum is shown. The truncated signal from the hyperpolarized [1,4-^{13}C]fumarate is at 176.1 ppm, the signals from carbon-1 and carbon-4 of [1,4-^{13}C]malate are at 182.5 and 181.3 ppm, respectively.

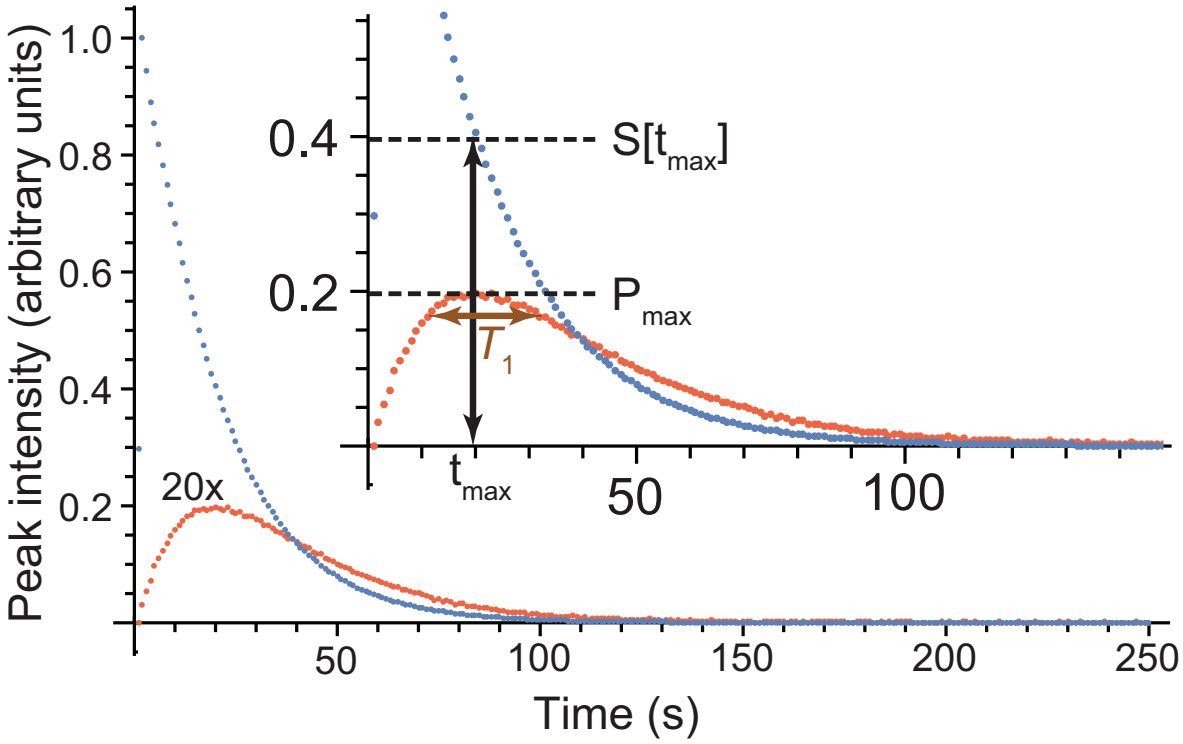

Figure 5. ^{13}C-NMR RD-DNP time courses obtained after injection of hyperpolarized [1,4-^{13}C]fumarate solution into a fresh hemolysate (final *Ht* = 42.5% and 22.2 mM fumarate). The decaying fumarate signal was normalized to a maximum of 1.0, while the signal from L-malate was scaled up by a factor of 20 to make it more visible on the given scale. The various lines and arrows were used in FmR_α analysis as described in the text. They yielded the estimates of the average T_1 = ~18 s and k_1 = ~1.4 × 10^{-3} s^{-1}.

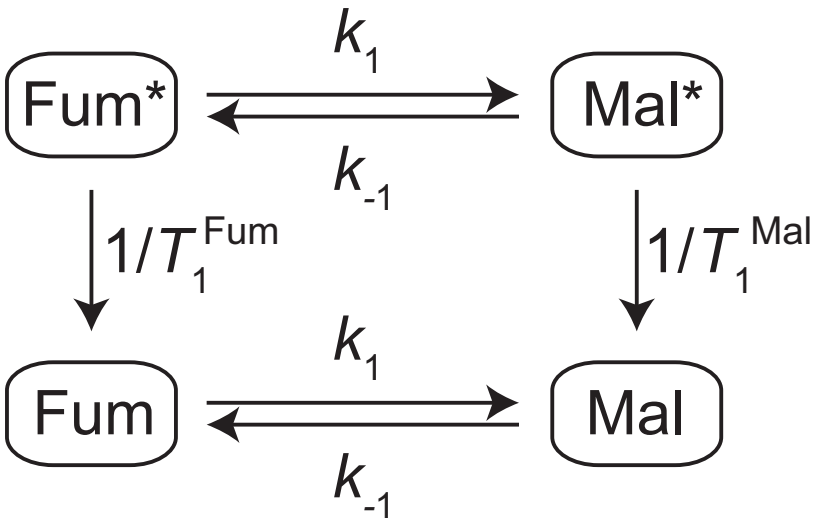

Figure 6. A kinetic scheme of the fumarase reaction in the ^{13}C-NMR RD-DNP experiment. The asterisks indicate hyperpolarized ('labelled') fumarate and malate species. The scheme served as a basis for modeling of the kinetics equations (Equations 7-10), which were used for the quantitative description of the RD-DNP experiment.

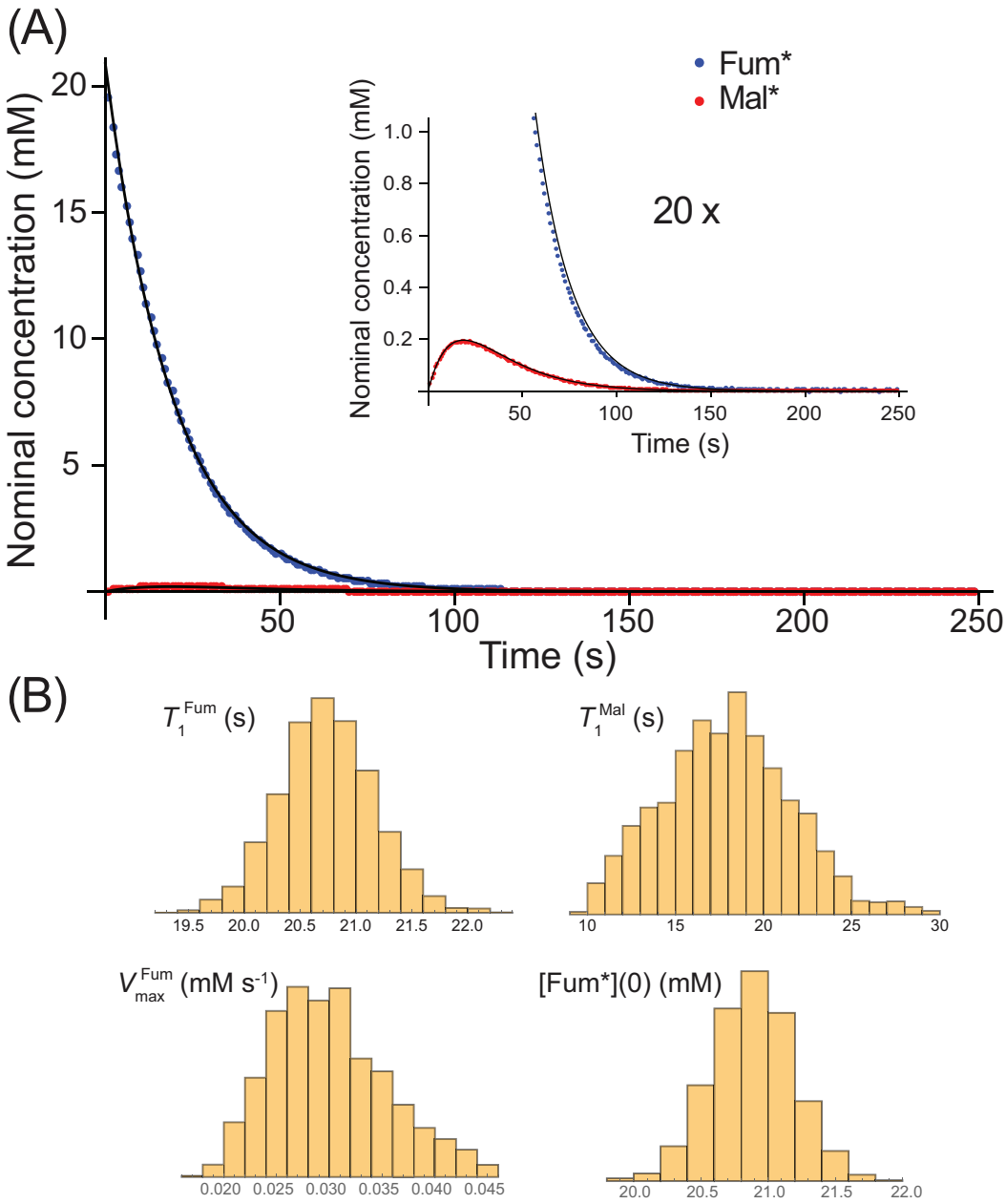

Figure 7. MCMC fitting analysis of ^{13}C-NMR RD-DNP data. (A) Time course of the nominal concentrations of the hyperpolarized fumarate (Fum*; blue dots), hyperpolarized malate (Mal*; red dots) and the fitted curves (solid black lines). 2.0 mL of hyperpolarized [1,4-^{13}C]fumarate solution was injected into 2.0 mL of fresh hemolysate containing 0.25 mL of $^{2}H_2O$ saline (154 mM NaCl). The MCMC analysis was used to fit the numerical solution of Equations 13-16 to the data and returned the following values of parameters (after constraining $\alpha = 4^o$, $K_{eq} = 2.4$, and $K_m^{Fum} = 3.9$ µM): $T_1^{Fum} = 20.7 \pm 0.5$ s; $T_1^{Mal} = 19.1 \pm 3.4$ s; $V_{max}^{Fum} = 4.0 \pm 0.8$ mmol (L RBC)$^{-1}$ min^{-1}; $V_{max}^{Mal} = 13.0 \pm 4.7$ mmol (L RBC)$^{-1}$ min^{-1}; and initial concentration of [Fum*](0) = 20.9 ± 0.3 mM. (B) The MCMC 'sensitivity analysis', presented as selected histograms illustrating the statistical variation in the fitted parameters (see text).